

3D IMAGING AND FLOW CHARACTERIZATION OF THE PORE SPACE OF CARBONATE CORE SAMPLES

Mark Knackstedt^{1,2}, Christoph Arns¹, Abid Ghous^{1,2}, Arthur Sakellariou¹, Tim Senden¹, Adrian Sheppard¹, Rob Sok¹, Holger Averdunk¹, W. Val Pinczewski², Girija S. Padhy³ and Marios A. Ioannidis³

(1) Australian National University, Canberra, Australia; (2) University of NSW, Sydney, Australia; (3) University of Waterloo, Waterloo, Canada.

This paper was prepared for presentation at the International Symposium of the Society of Core Analysts held in Trondheim, Norway 12-16 September, 2006

ABSTRACT

Carbonate rocks are inherently heterogeneous having been laid down in a range of depositional environments and having undergone significant diagenesis. They are particularly difficult to characterise as the pore sizes can vary over orders of magnitudes and connectivity of pores of different scales can impact greatly on flow properties. For example, separate vuggy porosity in an underlying matrix pore system can increase the porosity, but not the permeability and lead to large residual oil saturations due to trapping in vugs. A touching vug network can have a dramatic effect on permeability and lead to higher recoveries. In this paper we image a range of carbonate core material; from model carbonate cores to core material from outcrops and reservoirs via 3D via micro-CT.

Image-based calculations of porosity, MICP and permeability on 3D images of the carbonate systems are directly compared to experimental data from the same or sister core material and give good agreement. The carbonate systems studied include samples with well connected macroporous systems and other where the macroporosity is poorly connected. Simulation of permeability on these systems and direct analysis of local flow properties within the system allows one to directly illustrate the important role of the connectivity of macropores on flow properties. Pore network models generated from the images illustrate the varied topology obtained in different carbonate samples and show a dramatic difference when compared to clastic samples.

Many carbonate samples can include a significant proportion of microporosity (pores of 2 microns or less in extent) which are not *directly* accessible via current micro-CT capabilities. We discuss how one can map the structure and the topology of microporous regions crucial in studies of flow, production and recovery in carbonates. A hybrid numerical scheme is developed to measure the contribution of microporosity to the overall core permeability. Overall these results show the important role of identifying the connectivity of the pore sizes in dictating the single phase flow properties. Implications to two phase relative permeability and recovery are briefly discussed.

INTRODUCTION

Carbonate reservoirs contain more than 50% of the world's hydrocarbon reserves. In carbonate rocks, the processes of sedimentation and diagenesis produce microporous grains and a wide range of pore sizes, resulting in a complex spatial distribution of pores and pore connectivity. A reliable petrophysical interpretation for predicting the transport properties and producibility of carbonates is lacking.

Much of the poor reliability in estimating carbonate properties is due to the diverse variety of pore types observed in carbonates. Unlike sandstones, many carbonate sediments have a bi- or tri-modal pore size distributions with organisms playing an important role in forming the reservoirs. Carbonate rocks are further complicated by the significant diagenesis occurring through chemical dissolution, reprecipitation, dolomitization, fracturing, etc. For these reasons the size and shape of any porous network is expected to be very heterogeneous and exhibit pore sizes ranging from sub-micron to meters. In previous work we have described the development of a capacity to characterize and predict petrophysical properties from experimental 3D images of clastic rock microstructures from microtomographic images (Arns et al., 2005). Data derived from fragments of a range of cores including homogeneous and reservoir sands have been compared with conventional laboratory measurements and shown to be in good agreement (Arns et al., 2001, Arns et al., 2004, Arns et al., 2005b). In this paper model, outcrop and reservoir carbonate core plugs are imaged in 3D over a range of length scales using high resolution X-ray microtomography (μ CT). Image based calculations of petrophysical properties are compared with experimental data and show good agreement. High resolution numerical simulations of single phase flow and solute transport are undertaken on the resolved digital image data. Pore network models generated from the images illustrate the varied topology and geometry observed in carbonate samples.

Most reservoir carbonates exhibit a substantial presence of sub-micron porosity. Although pores at the submicron scale are not directly accessible via our current micro-CT capabilities one can investigate the regional distribution of microporosity via a chemical contrasting technique on the micro-CT facility. From the microporous mapping one can visualise the spatial distribution of the vuggy/macro/micro porosity contributions. The submicron pore structure can then potentially be resolved via Focused Ion Beam technology. The role of microporosity in the flow fields is illustrated via 3D visualisation, measurement of local flow velocities and solute transport results.

PROCEDURES

Images of the samples were captured on the ANU μ CT facility (Sakellariou et al., 2004, 2004a). These images, comprising up to 2000^3 voxels each, were filtered with anisotropic diffusion and segmented using the technique of converging active contours (Sheppard et al., 2003). Four samples are considered in this paper:

Samples 1 & 2: Two artificial vuggy carbonates samples are considered. These samples are created by consolidating monodisperse glass beads and CaCO_3 particles of different sizes in an oven, and then dissolving the carbonate particles by flowing acid (Padhy et al., 2005). Orthogonal slices of the two samples are shown in Figure 1. The first sample SC4 shows a high porosity intergranular medium decorated with large vugs. The second sample, SC16, no longer exhibits a granular structure; the “matrix” phase is made up of spherical pores, reminiscent of a vesicular rock, again decorated with vugs. In the center of the image we note the presence of undissolved CaCO_3 particles.

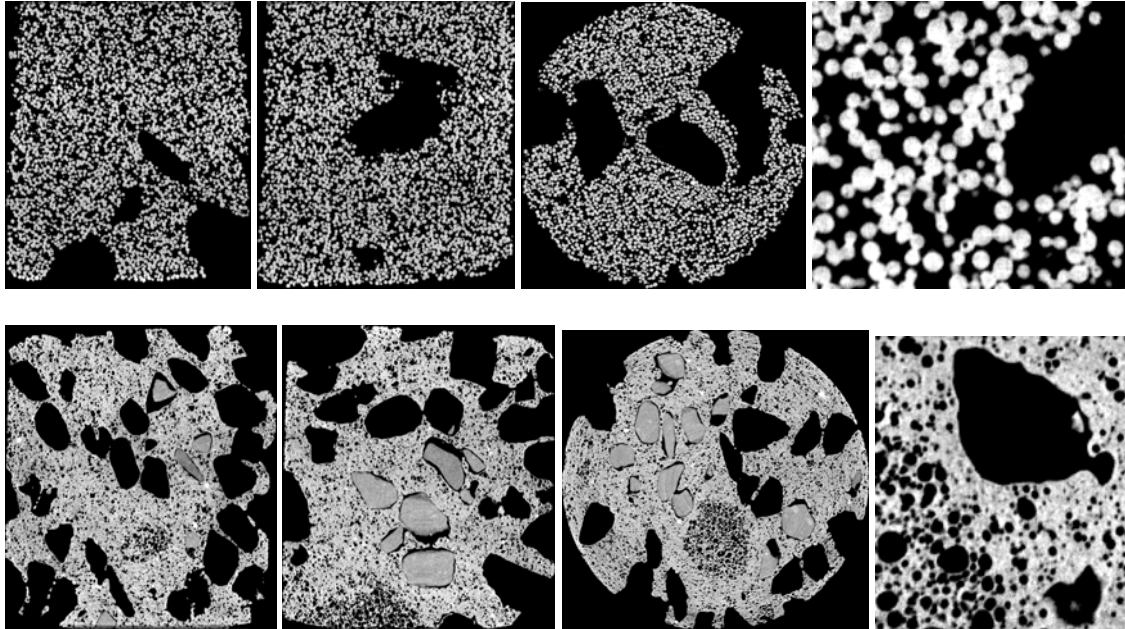


Figure 1: Original (grey scale) tomographic data for model carbonate samples. Upper row: Three orthogonal images of SC4 and (right) zooming in to grain level: Lower row: Three orthogonal images of SC16 and (right) zooming in on a vug/matrix region. Note the presence of partially dissolved and undissolved CaCO_3 particles in the center of the image volume.

Sample 3: Gambier limestone is a Oligocene-age outcrop quarried limestone from Mt. Gambier (MG), Australia. Air permeabilities and porosities measured on this sample respectively fall in the range of 4-10 Darcies and 50-55%. The limestone is composed of readily identifiable coral fossil fragments with a minor amount of coarse sparry calcite. A slice from the tomographic image of the core is shown in Fig. 2(a). The tomographic image is captured on a 5.5 mm diameter piece at 3.02 micron resolution. The resultant 3D pore structure is very complex exhibiting a broad range of pore and throat sizes. Waterflood recovery data under varying wettability conditions and flooding rates (Tie & Morrow, 2005) have been measured on core material from this formation.

Sample 4: A sample from a West Texas (WT) field was considered (Hidajat et al, 2004). This sample is clumpy in appearance with no clear depositional texture evident. A large amount of intergranular porosity is evident leading to higher permeabilities in regions. This sample is imaged at 3 different resolutions. First a 2 cm sample was imaged at 11.2

micron resolution, where some pores are evident (Fig. 2(b)). A second image at 6.04 micron resolution (1.1 cm sample) allows one to discern macroscopic interconnected porosity, but smaller details are still washed out of the image (Fig. 2(c)). A 5 mm subset was then imaged at 2.6 micron resolution where the connected porosity is strongly evident and local pore features are more clearly observed (Fig. 2(d)).

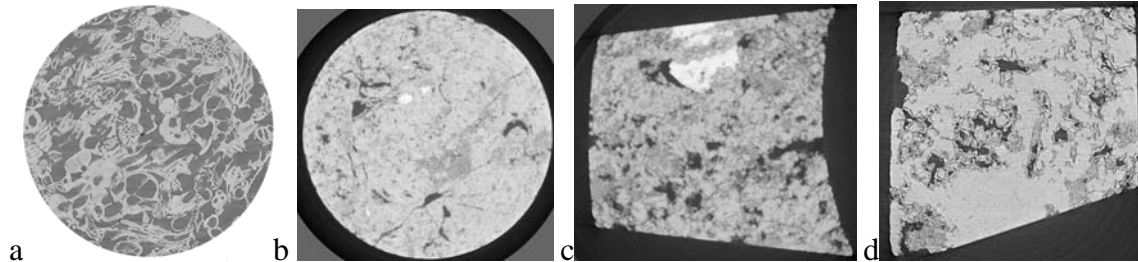


Figure 2: Slices through tomographic images of (a) Gambier limestone and images of WT carbonate at (b) lowest, (c) intermediate and (d) highest resolution.

Sample	Voxel (μm)	Image size	ϕ_{exp} (%)	ϕ_{image} (%)	k_{exp} (mD)	k_{image} (mD)	$l_c(x/y/z)$ (μm)
SC4	4.93	2000^3	48.4	53.2	7140	10000	89.2 / 75.8 / 90.8
SC16	4.89	2000^3	30.1	28.8	2400	700	25.3 / 53.0 / 72.8
MG	3.024	2000^3	54.0	51.3	2000-10000	4500	65.6 / 66.8 / 66.8
WT ₁	11.0	2000^3	23.4	3.5	n.a.	n.a.	n.a.
WT ₂	6.1	2000^3	23.4	5.5	n.a.	n.a.	n.a.
WT ₃	2.604	2000^3	23.4	8.5	140	124	14.7 / 26.5 / 9.0

Table 1: Image derived and experimental information on the 4 samples considered in this study. l_c , a critical pore diameter corresponding to the diameter of the smallest pore of the set of largest pores that percolate through the image is reported—if this value is significantly larger than the voxel size, one would expect to obtain good prediction of petrophysical data (Bauget et al., 2005). l_c is given in three orthogonal directions; variations in values indicate core heterogeneity.

RESULTS

MICP: DIGITAL vs. EXPERIMENTAL: A quality control step on the image data can be undertaken by comparing MICP measurement on the imaged core material to simulations of MICP undertaken directly on the images. Drainage simulations can be performed directly on voxelated images by defining locally for every voxel within the structure, the diameter of the largest sphere which fully lies within the pore phase and covers that voxel (Hilpert & Miller, 2001). At a fixed capillary pressure (pore entry radius) we consider all the spheres which have radius greater than or equal to the equivalent pore entry radius. Starting with the largest sphere and incrementing the sphere radius downwards (equivalent to incrementing capillary pressure upwards), the non-wetting phase saturation is measured as the subset of all spheres that have invaded the pore space. This results in a capillary pressure / equivalent pore radius vs. saturation

($P_c/r:S$) curve for the imaged core. This can be directly compared to experimental MICP data on the same (Gambier and WT) or sister (SC4 and SC16) core material. We find in all cases good agreement between the experimental and image-based results. In Fig. 3 we show the comparison between the image based and experimental data for the four core samples. In all cases the numerical fit to the experimental curve is good. For the SC4 and SC16 samples the experimental data starts at a non-zero saturation as only pores of diameter 180 microns or less are probed via MICP (1 psi entry pressure). The image data has a necessary cut-off at porosities associated with pores below image resolution. The Mt. Gambier image captures most of the porosity within the sample. In contrast, the intermediate West Texas sample exhibits most experimental porosity in the 0.5-3 micron pore size range (below image resolution). This match between experimental and numerical data gives one confidence in the quality of the 3D image data.

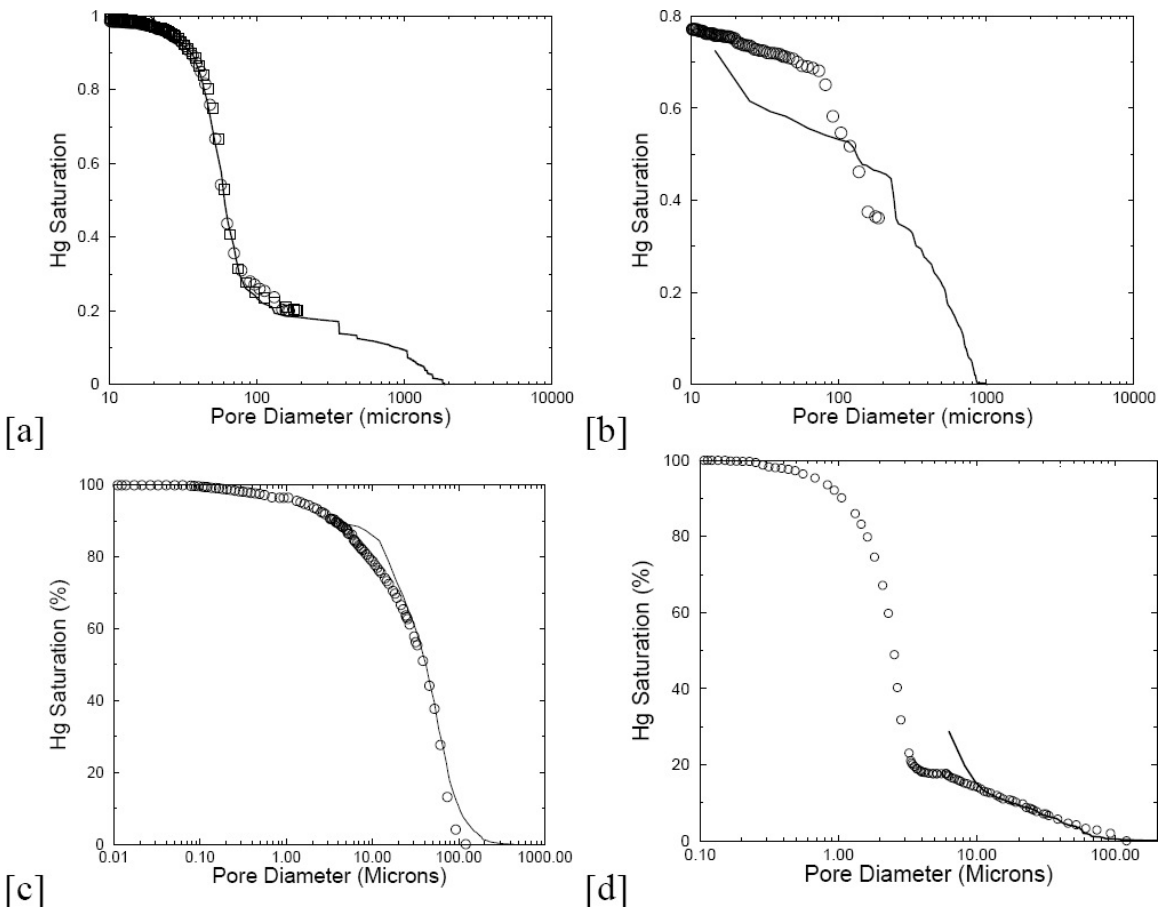


Figure 3: Experimental vs. Numerical MICP data for the 4 carbonates in this study. Experimental MICP data is given by the data points and the image based numerical data is given by the solid line. (a) SC4A showing two experiments and (b) SC16A. For both model carbonates the experimental data has been renormalized due to significant Hg invasion into vuggy porosity at the boundary before data recording. The poorer match to SC16 may be associated with core heterogeneity. (c) Mt. Gambier Limestone and (d) West Texas carbonate.

SINGLE PHASE FLOW RESULTS: A microstructure defined by a digital image is already discretized and lends itself immediately to numerical computation of many properties. In this paper we focus on the single phase permeability of the rock. The permeability calculation is based on the Lattice Boltzmann method (LB); details of the method have been previously described (Arns et al, 2004). Estimation of the permeability are made on the samples where the connected porosity is directly resolved on the tomograms (SC4, SC16, Mt. Gambier and high resolution WT). The results are summarized in Table 1 and agree reasonably well with experimental data.

PORE NETWORK IMAGES: Network models are considered as practical reservoir description and simulation tools to study a variety of two- and three-phase displacement processes. To date network models used for the study of multiphase flow have been based on idealized networks (Bryant et al., 1993, McDougall et al, 2002) or are generated by stochastic realizations based on thin section data and/or MICP data (Bakke & Oren, 1997). This work has been primarily limited to clastic samples. The description and validation of robust techniques for partitioning the pore space of a porous material and descriptions of the methods used to generate the network are beyond the scope of this paper and are given elsewhere (Sheppard et al., 2005; Sheppard et al., 2006). Here we show that the networks generated directly from the 4 microtomographic images of carbonates exhibit a strongly varying topology and pore geometry and are distinctly different to networks generated on clastic images.

In Figure 4 we show 4 images of network subsets; one derived directly from a 3D image of a simple sandstone (Castlegate), and three derived from the carbonate images; one model carbonate (SC16), one outcrop carbonate (Mt. Gambier) one high resolution reservoir (West Texas) carbonate. The networks in Fig. 4 contain less than 4% of the full image volume obtained from the full tomogram. The difference in the network structure between the carbonate and clastic samples is clear and the visual differences across the three carbonate samples is also dramatic.

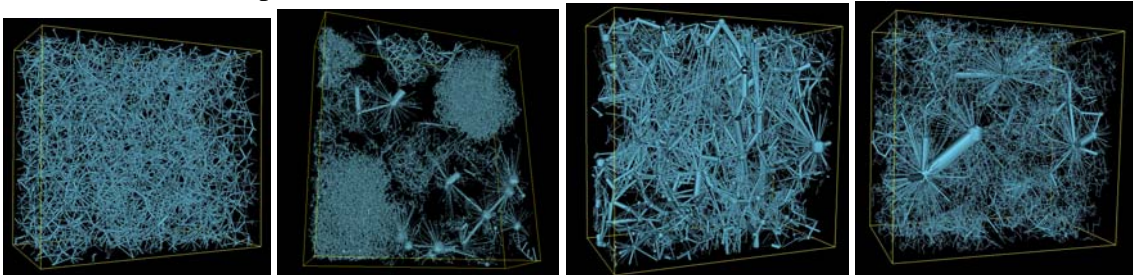


Figure 4: Networks of (from left to right) Castlegate sandstone ($520^2 \times 230$ subset), SC16 ($1120^2 \times 1224 \times 325$ subset), Mt. Gambier limestone and West Texas carbonate (last two samples are $660^2 \times 320$ subsets of the original sample). The size of the pores and throats reflects their actual size in the partitioning of the 3D image. The variation in structure across the 3 samples is dramatic.

	N_t	N_p	Z_m	Z_w	Z_{max}	$(R_p/R_t)_m$	$(R_p/R_t)_w$
CS	272422	102682	5.4	9.0	49	2.9	4.0
SC16	83047	46171	3.6	31.4	227	3.0	30.3
MG	149055	51333	5.6	30.0	372	6.5	20.3
WT	131245	67863	3.8	35.0	276	3.4	28.0

Table 2: Details of the network structure for the five samples shown in Fig. 4. Z_m gives the mean coordination number, Z_w the volume weighted mean and Z_{max} the maximal pore coordination number. The mean $(R_p/R_t)_m$ and volume weighted $(R_p/R_t)_w$ pore to throat aspect ratios are also given.

From the images a number of important network parameters can be ascertained; two of the more important parameters are the coordination number of the pores in the network Z and the aspect ratio of the pore radii (R_p) to the throat radii (R_t). Mean data and data weighted by pore volumes are given in Table 2. We observe that despite the varying topology, the mean Z of the sandstone and Mt. Gambier are similar, while the West Texas and model carbonates are higher. The weighted coordination number is however much larger for all carbonates (>30) reflecting the strong interconnectivity of the larger pores. The mean aspect ratio is ~ 3 in three of the four samples; the Mt. Gambier system exhibits a significantly larger mean aspect ratio. However, the volume weighted aspect ratios are highest for the two other carbonates, and all are significantly larger than observed for the sandstone. The volume weighted data highlights the important differences exhibited by carbonate networks compared to their clastic counterparts; e.g., aspect ratio can strongly affect the multiphase flow properties (see Nguyen et al., 2006) of core material.

Microporosity Imaging: As seen in Fig. 3(d), microporosity, pores at the submicron scale are not directly accessible via our current micro-CT capabilities. The presence of microporosity in carbonates is well documented. Visual representation of the micropore structure in carbonates is given, for example, in Cantrell & Hagerty, 1999. This microporosity plays a key role in understanding rock properties. In this subsection we discuss imaging methods for considering microporosity in carbonates including methods to potentially map the structure and the topology of microporous regions to better understand flow, production and recovery data. We also describe preliminary results of a method to visualise the topology of microporous regions.

To observe the partitioning of microporous regions within a sample we undertake two experiments on a small subset (6mm diameter) of the West Texas carbonate at low/intermediate resolution (in this case 8.4 microns). In the first experiment we obtain a dry image. We then undertake drainage experiments within the μ CT with X-ray opaque fluids. Drainage to pore sizes in the submicron range will allow discrimination of pathways which connect the larger (resolved) porosity at different scales. To date we have not undertaken a full drainage experiment, but have undertaken a study on a dry and then completely saturated sample. In Fig. 5(a) we show a slice of the system under wet conditions and the predicted regions of microporous rich material after phase separation.

In this sample we measure ~3% resolved porosity, and ~20% total porosity where we use the CT density of the wet-dry image to estimate local porosity contributions. The measured porosity of the sample from He and Hg porosimetry is 23%. A 3D visualisation of the macroporous, microporous rich and matrix phase from a small subset of the image (128 x 256 x 395) is shown in Fig. 5(b).

Ongoing work includes the tomographic imaging of these "nested" microporous regions via higher resolution tomographic imaging methods (e.g, Focused Ion Beam (FIB) tomography and laser confocal imaging). To date we have used FIB technology; FIB allows for the milling of layers as thin as 10 nanometres. After each milling step a new surface is exposed and a 2D image of the surface can be generated. By serial stacking of the 2D images a 3D reconstruction can be generated. 2D images of the West Texas carbonate sample at submicron resolution are given in Fig. 6. The detailed information from higher resolution methods should allow one to populate the topology of the microporous regions with realistic and detailed pore geometry information.

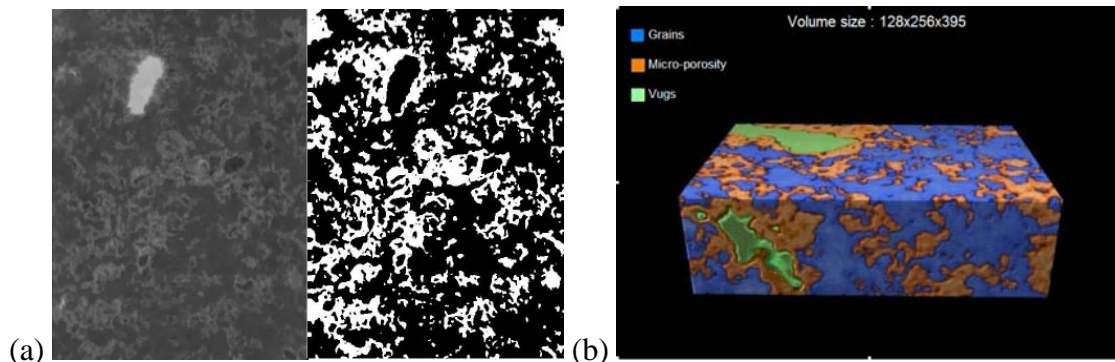


Figure 5: (a) Snapshot of the microporosity rich regions from one slice of the tomogram. (Left) shows the attenuation map with the bright spot in upper left a large (resolvable) pore; Right shows the image after phase separation where the perceived microporous rich region is shown in white; matrix and resolved macropores are given in black. (b) Snapshot from a 3D visualization of a large pores (green) and the connectivity via microporosity.

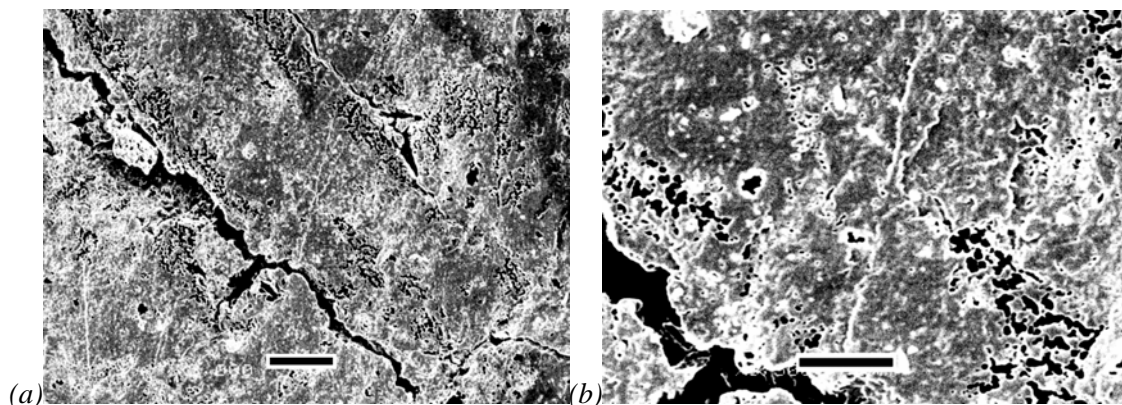


Figure 6: SEM images of FIB prepared surfaces of the West Texas carbonate (a) Scale bar is 5 microns and (b) scale bar is 2 microns. Note the presence of significant porosity in the range 0.5-3 microns as observed in the MICP data for this sample (recall Fig.3 (d)).

Incorporation of Microporosity into Transport Calculations: Given the importance of microporosity to the overall properties of carbonates, there is a need to undertake a study of the transport properties of the core material incorporating both the resolvable porosity and the microporosity. It is impossible to simultaneously solve for properties of microporous carbonate systems incorporating all the microstructural features of the carbonate due to the varying (hierarchical) length scales which collectively contribute to transport. However, one can use the division of the carbonate into two regions as described experimentally; (1) the larger resolved pores and (2) the regions of microporosity. In the larger pores the Stokes' equations for incompressible flow are solved. Regions with the smaller unresolved pores are described by Darcy's law where one must input the effective permeability of the microporous regions. The two boundary conditions to be satisfied at the macropore / micropore interface are continuity of the fluid velocity and shear stress. The Brinkman equation, a generalization of Darcy's law facilitates the matching of boundary conditions between the larger pores and the permeable medium. Although the Brinkman equation is semiempirical, it has been validated by a detailed numerical solution of the Stokes' equations in regions near the interface between regions of dissimilar permeability. It is relatively straight forward to integrate this approach into a standard lattice-Boltzmann solver (Martys, 2001).

We study both the flow fields and the dispersion of a neutral tracer through the system. The movement of a tracer in a fluid flow field is, at the pore scale, defined by a balance between diffusion and convection in the asymptotic dispersion regime (both diffusion and convection contribute). Given the solution of the Stokes or Brinkman equation, we consider a stochastic process on this velocity field to solve the diffusion-advection equation using a random walk technique (Makse et al., 2000) in 3D. We introduce a large number of walkers at the inlet, and then simulate each trajectory until the walkers reach the outlet, resulting in 100% recovery of the tracer. In Fig. 7 we show the neutral tracer residence time distributions for the resolvable porosities for the Gambier and WT carbonate images at varying flow rates. Both exhibit a significant broadening of the distribution with decreasing flow velocity.

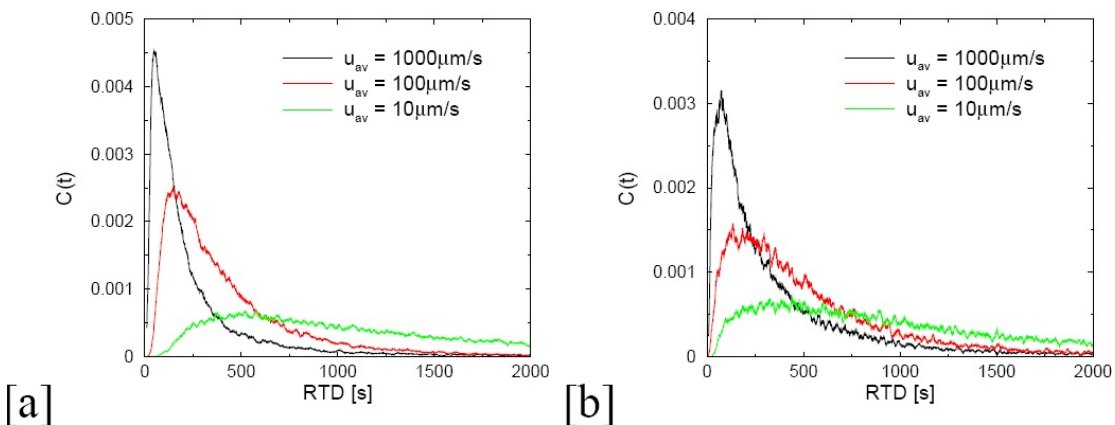
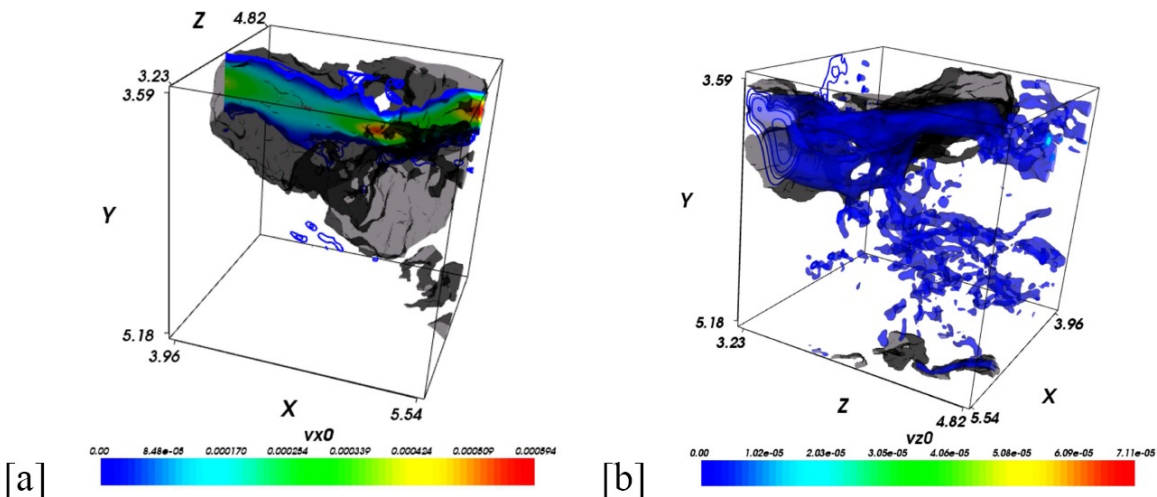


Figure 7: Neutral tracer residual time distributions for delta pulses and different flow fields calculated by solving the diffusion-advection equation in the resolved pore spaces of subsections of the four carbonate rocks: (a) SC4, (b) SC16, (c) Gambier limestone (300^3), (d) High resolution WT carbonate (300^3).

The role of microporosity on the flow field of the WT carbonate is illustrated in Fig. 8. The inclusion of microporosity can lead to a more dispersed flow field (when macropores are poorly connected). The effect of microporosity on RTDs will be considered in future work.

One can also directly measure the pore scale flux analysis from image data; measure the velocity field for the flow of an incompressible fluid through the structure defined by a tomogram. This is done by directly calculating the flux between two neighbouring voxels as the projection of the velocity between those voxels. From the partitioning of the pore space (recall Fig. 4) into pore bodies and throats one can measure the flux across pores (q_p) within the image. In Fig. 9 we show a plot of the flux within local pores from the partitioning of the WT sample and a Castlegate sand sample. We normalise the local pore flux by the total flux across the sample volume (q_t). The carbonate exhibits a much broader distribution of local flux with pore size (a variation of over 5 orders of magnitude in relative flux for pores of the same size) and exhibits many pores where all or most of the flow is concentrated ($q_p/q_t \sim 1.0$). In contrast the Castlegate data shows a smaller variation in local flux distribution with pore size and $(q_p/q_t)_{\max} \sim 0.10$. This high variability in local flow velocities and the potential for focusing of the flow through a small subset of the pores illustrates the effect of the poor connectivity of larger pores on flow properties in carbonates.



[a] **[b]**
 Figure 8: Calculation of flow fields for a subsection of the West Texas carbonate sample imaged in the microporosity study (Figure 5) using the Brinkman equation: Subsample size = 200^3 , Voxel size = 8.4 microns). We choose two flow directions. [a] flow along x-axis where a resolvable macroporous cluster connects and therefore the velocity field is dominated by the macroporosity; indicated by a contour plane. [b] flow in an orthogonal direction (along z axis) where the only permeable pathway is through the microporous region, the velocity field is now slower and more dispersed; indicated by a connecting velocity iso-surface. In both figures the grey surfaces indicate the resolved macroporosity.

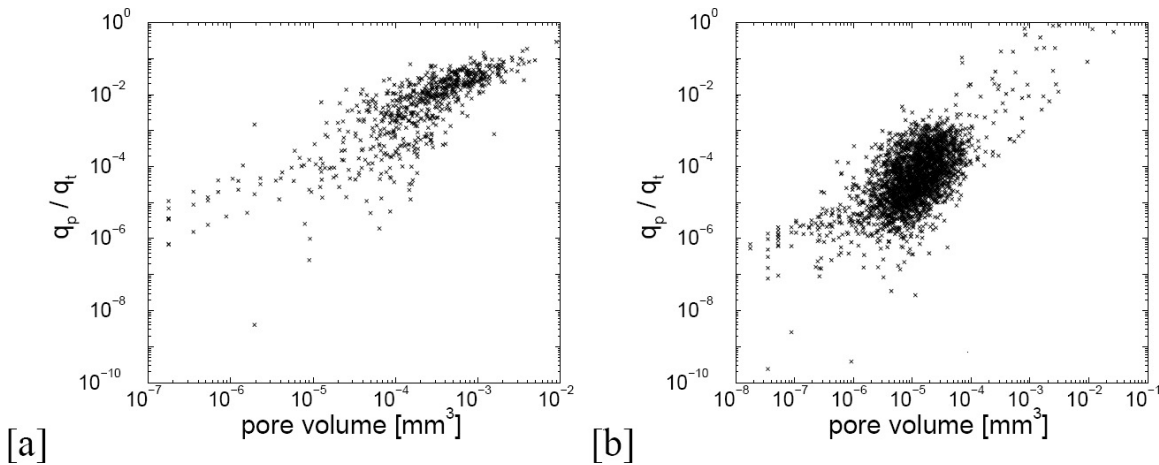


Figure 9: Local flux per pore as a function of pore size for (a) Castlegate sandstone and (b) WT carbonate.

CONCLUSIONS & DISCUSSION

- A set of carbonate core samples has been imaged in 3D across a range of resolutions. The resultant 3D pore structure exhibits extremely strong variations across samples. The contribution to porosity and 3D connectivity of pores at different length scales is examined.
- Porosity and MICP measurements performed on the imaged core material are in good agreement with image-based MICP simulations. Permeability from image data is in reasonable agreement with experiment.
- Pore network models generated from the images illustrate the large variations in topology and geometry observed in carbonate samples. Both the visual appearance and quantitative details of the pore network show dramatic differences to networks derived from clastic images.
- The topology of the microporous phase (pores below image resolution) is probed via a chemically-based X-ray contrasting technique. Focussed Ion Beam SEM may allow the 3D resolution of cores at submicron scales.
- High resolution numerical simulations of single phase flow and solute transport are undertaken on the resolved digital image data. A hybrid numerical scheme is developed to include the contribution of microporosity to the overall core permeability.

In parallel work (Nguyen et al, 2006), two phase imbibition properties have been compared for networks based on clastic and carbonate images. Results show the strong dependence of two phase imbibition flow properties on topological and structural properties of the pore network. Petrophysical units, or rock types, are defined to help petrophysicists and reservoir engineers assign petrophysical characteristics to different zones of a reservoir. Porosity, permeability, grain density, mercury injection capillary pressure curves are often used as markers of the type of porous rocks. Rocks are clustered into groups based on these measures; these groups are assumed to have similar flow and

storage capacity. Facies are identified using depositional and diagenetic criteria which are tied to poro-perm data. Relationships are used to tie the petrophysical to the geological models along with log typing to estimate initial hydrocarbons in place. It is also frequently assumed that the rock types defined by this process are valid to assign two-phase flow characteristics (e.g. relative permeability) independent of the recovery process. Recently, however, it has been shown (Hamon, 2003) that conventional rock typing methods may not capture the actual variability of relative permeability curves and that there is no systematic correspondence between rock types used to estimate hydrocarbons in place and those required to describe production behaviour. The application of 3D imaging and analysis technology to rock cores will certainly aid the development of improved cross-property correlations. Excitingly, the development of libraries of 3D images will allow a more rigorous and quantitative description of rock type and texture of carbonates and clastics. This should, in turn, give one the potential to more fully integrate classical and dynamical rock typing methods; sedimentological descriptions, elastic behaviour, poro-perm trends, capillary pressure data and saturation functions to relative permeability and residual saturations

REFERENCES

- Arns, C.H., M.A. Knackstedt, W.V. Pinczewski, and W.B. Lindquist (2001): "Accurate Computation of transport properties from microtomographic images." *Geophysical Research Letters* **28**, 3361-3364.
- Arns, C.H., M.A. Knackstedt, W.V. Pinczewski, and N. Martys (2004): "Virtual permeametry on microtomographic images." *J. Petroleum Sci. and Eng.* **45**, 41-46.
- Arns, C. H., F. Bauget, A. Ghou, A. Sakellariou, T. J. Senden, A. P. Sheppard, R. M. Sok, W. V. Pinczewski, J. Kelly, and M. A. Knackstedt (2005): "Digital core laboratory: Petrophysical analysis from 3D imaging of reservoir core fragments", *Petrophysics*, 46, 260-277.
- Arns, C.H., A. Sakellariou, T.J. Senden, A.P. Sheppard, R.M. Sok, W.V. Pinczewski, P.E. Oren, S. Bakke, L.I. Berge, and M.A. Knackstedt (2005b): "Pore scale imaging of Carbonates." *SPEJ*, 475-484.
- Bakke S, P. Oren, "3-D pore scale modelling of heterogeneous sandstone reservoir rocks and flow simulations in the pore networks", *SPE* (1997) 35479.
- Bauget, F, Arns, C, Sheppard, A, Sok, R, Pinczewski, V., Knackstedt, M., Rock Typing and Petrophysical property estimation via direct analysis on microtomographic images, *Proceedings of the Annual Symposium of the Society of Core Analysts*, SCA2005-81, Toronto, Canada.
- Bryant S.L., D. W. Mellor, C. A. Cade (1993): "Physically representative network models of transport in porous media", *AIChE Journal*, **39**, 387
- Cantrell, D. L., and Hagerty, R. M., 1999: "Microporosity in Arab Formation Carbonates, Saudi Arabia": *GeoArabia*, **4**, 129-154.
- Hamon, G. (2003): "Two Phase Flow Rock Typing", *Society of Petroleum Engineers, Proceedings of the 2003 Annual Technical Conference & Exhibition*, SPE 84035, Denver, Colorado.
- Hidajat, I., Mohanty, K. K., Flaum, M. and Hirasaki, G. (2004): "Study of vuggy carbonates using nmr and x-ray ct scanning", *SPE Reservoir Evaluation and Engineering*, pages 365--377.
- Hilpert, M., and C. T. Miller (2001): "Pore-morphology based simulation of drainage in totally wetting porous media", *Adv. Water Res.* **24**, 243-255.
- Makse, H, J. Andrade and H. E. Stanley (2000): "Tracer dispersion in a percolation network with spatial correlation, *Phys. Rev. E*, **61**, 581-586.
- Martys, N. S. (2001): "Improved approximation of the Brinkman equation using a lattice Boltzmann method", *Physics of Fluids*, **13**, 1807-1810.
- Martys, N. S., Torquato, S. and Bentz, D.P. (1994): "Universal scaling of fluid permeability for sphere packings" *Phys. Rev. E*, **50**, 403.

- McDougall SR, Cruickshank J., and KS Sorbie (2002): "Anchoring methodologies for pore-scale network models: application to relative permeability and capillary pressure prediction", *Petrophysics* **43**, 363-375.
- Nguyen, V., Sheppard, A, Knackstedt, M and Pinczewski, W.V (2006): "Micro-CT Based Network Model Predictions of Imbibition Relative Permeability and Residual Saturations", *Proceedings of the Annual Symposium of the Society of Core Analysts*, SCA2006, Trondheim, Norway.
- Padhy, G., M. A. Ioannidis and C. Lemaire (2005): "Special Core analysis studies in Vuggy porous media of controlled microstructure", *Proceedings of the Annual Symposium of the Society of Core Analysts*, SCA2005-76, Toronto, Canada.
- Sakellariou, A., T.J. Senden, T.J. Sawkins, M.A. Knackstedt, A. Limaye, C.H. Arns, A.P. Sheppard, and R.M. Sok (2004): "An x-ray tomography facility for a wide range of mesoscale physics applications." U. Bonse (ed.): *Proceedings of SPIE* **5535**. Bellingham, WA, pp. 166-171
- Sakellariou, A., T. J. Sawkins, T. J. Senden and A. Limaye (2004a): "X-ray tomography for mesoscale physics applications", *Physica A*, 339, 152-158
- Sheppard, A. P., R. M. Sok and H. Averdunk (2004): "Techniques for image enhancement and segmentation of tomographic images of porous materials", *Physica A*, 339, 145-151
- Sheppard A. P., R. M. Sok, H. Averdunk (2005): "A new method for the extraction of pore networks", *Proceedings of the Annual Symposium of the Society of Core Analysts*, SCA2005-20, Toronto, Canada.
- Sheppard A. P., R. M. Sok, H. Averdunk, V. Robins and M. Saadatfar(2006): "Analysis of Rock microstructure using high-resolution x-ray tomography", *Proceedings of the Annual Symposium of the Society of Core Analysts*, SCA2006, Trondheim, Norway.
- Tie, H., and N. Morrow(2005): "Low flood rate residual saturations in carbonates: Low flood rate residual saturations in carbonates", *Society of Petroleum Engineers, Proceedings of the International Petroleum Conference*, IPTC 10470, Doha, Qatar.